ELSEVIER

ISPRS Journal of Photogrammetry & Remote Sensing 56 (2002) 210–220

PHOTOGRAMMETRY & REMOTE SENSING

www.elsevier.com/locate/isprsjprs

Preserving cartographic quality in DTM interpolation from contour lines

G. Gonçalves [a,*], P. Julien [a], S. Riazanoff [b], B. Cervelle [b]

[a] *Laboratoire Matis, Service de la Recherche, Institut Géographique National, 2 Avenue Pasteur, 94160 Saint-Mandé, France*
[b] *Université de Marne-la-Vallée, 5 Boulevard Descartes, 77454 Marne-la-Vallée cedex 2, France*

Received 31 March 1999; accepted 18 January 2002

Abstract

Fitting an elastic grid to contour lines (CLs) produces a surface with tighter intermediate contours than the initial ones. This leads to intermediate contours that do not match the initial ones. In this paper, we propose a method for correcting this defect, by fitting the elastic grid to supplementary constraint lines that correspond approximately to the terrain morphologic lines (ridges and drainages). We extract these lines from a Delaunay triangulation consistent with the contour lines. We propose a coherent weighting system for the constraints imposed on the elastic grid. Finally, we show that a digital terrain model (DTM) artefact of the type mentioned above can be detected by a simple criterion such as the contour length.

Keywords: Contour lines; DTM; Interpolation; Elastic grid; Constraint lines; Delaunay triangulation; Voronoi diagram; Contour length graphs

1. The intermediate contours problem

In the context of research on the quality of digital terrain models (DTMs), we have been led to reconsider the problem of interpolating regular grid models from contour lines (CLs). For this purpose, we have already at our disposal the elastic grid method (D'Autume, 1978), which fits an elastic surface (a flexible plate) to a finite sample of points. The first use of the elasticity condition is to prevent, for any sample, the indeterminability of the problem; however, it also has the advantage of producing smooth surfaces. The elastic grid, which we review in Section 2, is the discrete equivalent of the thin plate spline (Duchon, 1976). These methods are now widely used, notably after (Grimson, 1981).

To fit an elastic grid to a set of contour lines (polylines in fact), one must first obtain a finite point sample for that data. Usually, these points are sampled directly from the CLs, using a sufficiently small sampling interval in order to make the sample representative. Such a sample is satisfying as long as the check is limited at superposing the initial contours with the corresponding contours computed from the fitted surface: the superposition is correct. The sample is less satisfying if one draws the intermediate contours of the fitted surface. In fact these contours are straighter than the initial ones, in the sense that they do not follow the initial CLs; this phenomenon is particularly perceptible at the ridge and drainage lines. Such intermediate contours are unacceptable since

* Corresponding author. Present address: Departamento de Matemática, Universidade de Coimbra, Apartado 3008, 3000 Coimbra, Portugal. Tel.: +351-239-791185; fax: +351-239-832568.
E-mail address: gil@mat.uc.pt (G. Gonçalves).

0924-2716/02/$ - see front matter
PII: S0924-2716(02)00044-8

their shape does not follow the contour line modelling principle, well known by cartographers, according to which one should always be able to consider that the slope between two consecutive or intermediate contours is regular.

Fig. 1 illustrates this problem for a synthetic surface: Fig. 1a and b shows the initial contours and the input sample. Fig. 1c shows the fitted surface contours, with the intermediate contours too tight. Lastly, in Fig. 1d, we show the intermediate lines following the contour line modelling principle.

These flaws are not specific of elastic surfaces; they also occur at ridge and drainage lines, when one interpolates a surface using a triangulation computed from contour lines (Robinson, 1994).

An analysis of the positions where these flaws occur indicates that information constraining the surface fitting was missing at the ridges and drainages. One is led to think that the correction of this problem will involve adding supplementary information to the interpolation method. We shall see in Section 3 that it is possible to extract this additional information from the contour lines, and to use it to construct a correct surface.

In addition, in Section 4, we will show that the presence of the above flaws may be easily detected, by comparing the initial and intermediate contour lengths.

2. Implementing the elastic grid

2.1. Description of the elastic grid method

An elastic grid fits a function $H(X,Y)$, representing the DTM, to a set of sampling points

$$S = \{(X_i, Y_i, Z_i); \quad i = 1, \ldots, n\}. \tag{1}$$

The function $H(X,Y)$ is assumed to be defined by means of an interpolation function defined on a

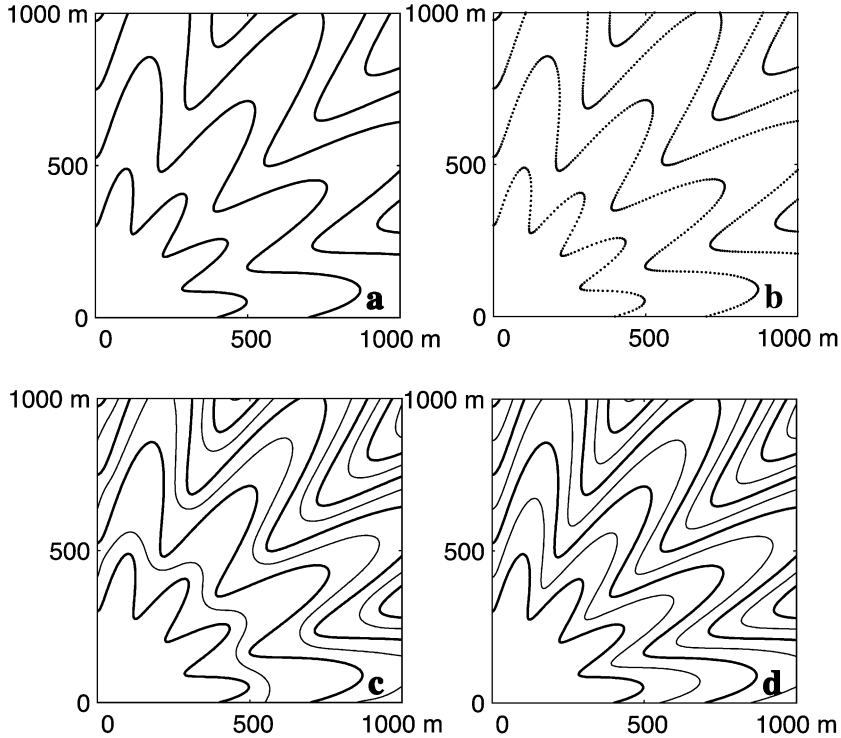

Fig. 1. The intermediate contours problem: (a) initial contours; (b) sample points; (c) initial contours (in bold) and intermediate contours of the fitted surface; (d) the same contours respecting the CL modelling principle.

regular square grid. In this paper, we assume it to be piecewise bicubic, and given by:

$$H(X,Y)=\sum_{c=1}^{N}\sum_{l=1}^{M}U\left(\frac{X-X_c}{h}\right)U\left(\frac{Y-Y_l}{h}\right)z_{c,l} \quad (2)$$

where N, M are the numbers of columns and rows in the grid, respectively, h its interval, $z_{c,l}$ the heights at grid points (X_c,Y_l) and $U(t)$ the piecewise polynomial interpolation function

$$U(t)=\begin{cases}\frac{3}{2}|t|^3-\frac{5}{2}|t|^2+1 & \text{if } 0\le|t|\le 1\\ -\frac{1}{2}|t|^3+\frac{5}{2}|t|^2-4|t|+2 & \text{if } 1<|t|<2\\ 0 & \text{if } |t|\ge 2\end{cases}. \quad (3)$$

The elastic grid defines H as the function minimizing:

$$E(H)=E_{\text{sample}}(H)+E_{\text{curvature}}(H) \quad (4)$$

where

$$E_{\text{sample}}(H)=\sum_{i=1}^{n}w_i[H(X_i,Y_i)-Z_i]^2 \quad (5)$$

and

$$E_{\text{curvature}}(H)=\frac{1}{h^2}\left[\sum_{c=2}^{N-1}\sum_{l=1}^{M}(z_{c-1,l}-2z_{c,l}+z_{c+1,l})^2+\sum_{c=1}^{N}\sum_{l=2}^{M-1}(z_{c,l-1}-2z_{c,l}+z_{c,l+1})^2+\frac{1}{8}\sum_{c=2}^{N-1}\sum_{l=2}^{M-1}(z_{c-1,l-1}-z_{c-1,l+1}-z_{c+1,l-1}+z_{c+1,l+1})^2\right].$$

In Eq. (5), w_i is a weight ($w_i>0$) associated to the point (X_i,Y_i,Z_i) to which we shall return in Section 2.3. The introduction of the term $E_{\text{curvature}}$ ensures the existence of one single solution whatever the point sample may be (see Section 2.4), whereas simply minimizing E_{sample} leads to an infinity of solutions if $NM>n$ (there are more grid points than sample points).

The name "elastic grid" comes from the physical interpretation that may be given to this method. One considers the mesh to be materialized by rigid bars connected to each other by elastic links. In absence of external forces, the bars are aligned to each other and this elastic surface models a plane. On the other hand, the sampling points are attached to the imaginary surface by vertical springs of rigidity w_i. $E(H)$ represents the energy of this structure. Minimizing the energy leads to the fitting surface: the structure has attained a position of equilibrium.

Notice that the expressions $(z_{c-1,l}-2z_{c,l}+z_{c+1,l})/h^2$, $(z_{c,l-1}-2z_{c,l}+z_{c,l+1})/h^2$, $(z_{c-1,l-1}-z_{c-1,l+1}-z_{c+1,l-1}+z_{c+1,l+1})/4h^2$, are respectively, finite difference approximations of the second derivatives $H_{XX}(X,Y)$, $H_{YY}(X,Y)$, $H_{XY}(X,Y)$. In this way, $E_{\text{curvature}}(H)$ is a Riemann sum approximating the integral

$$K(H)=\int\int_{\Omega}[H_{XX}^2(X,Y)+2H_{XY}^2(X,Y)+H_{YY}^2(X,Y)]\,\mathrm{d}X\,\mathrm{d}Y. \quad (6)$$

This integral characterizes thin plate spline surfaces, since they are known to minimize the expression $E_{\text{sample}}(H)+K(H)$ (Duchon, 1976). An elastic grid fitted surface is thus a discrete approximation of a thin plate spline surface.

It can be also shown that

$$H_{XX}^2(X,Y)+2H_{XY}^2(X,Y)+H_{YY}^2(X,Y)=K_1^2(X,Y)+K_2^2(X,Y) \quad (7)$$

where K_1, K_2 are the principal curvatures of the surface $\overline{H}=H-T$. This surface can be seen as the difference between H and its tangent plane at (X,Y), that is, $T(u,v)=H(X,Y)+H_X(u-X)+H_Y(v-Y)$, where H_X and H_Y are the first derivatives of H. This means that $K(H)$ is a measure of the "quadratic mean" curvature of surface $\overline{H}$. Since $\overline{H}$ actually contains all the curvature information of $H=\overline{H}+T$ (the plane has no curvature), one sees that $K(H)$ is a measure of the curvature in H. This explains the notation $E_{\text{curvature}}(H)$ for the quantity approximating $K(H)$.

2.2. Differences with respect to the D'Autume method

Compared to the method described in D'Autume (1978), we have introduced three modifications, which will be discussed below.

2.2.1. Rotation-invariant curvature

In D'Autume's method, $E_{\text{curvature}}(H)$ did not contain the term corresponding to H_{XY}. This means that $E_{\text{curvature}}(H)$ approximated the integral $\int\int H_{XX}^2 + H_{YY}^2\,\mathrm{d}X\mathrm{d}Y$ and not $K(H)$. Now, $K(H)=\int\int K_1^2+K_2^2\,\mathrm{d}X\mathrm{d}Y$ seems to be a more acceptable measure, since $K_1^2+K_2^2$ is a geometric property of the surface, independent of the coordinate system used.

2.2.2. Piecewise bicubic model

D'Autume's method also assumed the function $H(X,Y)$ to be piecewise bilinear, i.e., defined by means of the linear interpolation function $Q(t)=\sup(0, 1-|t|)$, instead of the cubic interpolation function $U(t)$. We prefer to define H by means of U to obtain a C^1 surface (with continuous first derivatives), useful for DTM applications that require slope computations. On the other hand, there exists an infinite family of differentiable cubic interpolation functions, indexed by the parameter a

$$V_a(t)=\begin{cases}(a+2)\,|t|^3-(a+3)\,|t|^2+1 & \text{if } 0\le|t|\le 1\\ a\,|t|^3-5a\,|t|^2+8a\,|t|-4a & \text{if } 1<|t|<2\\ 0 & \text{if } |t|\ge 2\end{cases}. \quad (8)$$

This parameter is nothing but the derivative $V_a'(1)$. From this family, we choose the function U because for any function $f(X)$ of class C^3 (with continuous derivatives of order three), $U=V_{-1/2}$ is the only function that gives a $O(h^3)$ interpolation error; any other V_a gives a $O(h)$ error (see Appendix A).

It can be also shown that, U is the only one for which the interpolation function g is exact if f is a polynomial of degree 1; furthermore, it is also exact for polynomials of degree 2 (Julien, 1994).

2.2.3. Inequality constraints on the grid point heights

At each grid point, we impose the following conditions on the surface H:

$$Z_1(c,l)\le H(X_c,Y_l)=z_{c,l}\le Z_2(c,l) \quad (9)$$

where $Z_1(c,l)$, $Z_2(c,l)$ are the heights of the two CLs surrounding the grid point (X_c,Y_l).

2.3. Weight assignment

Assigning correct values for the weights w_i is of extreme importance for the elastic grid. In fact, since the fitting function $H(X,Y)$ is defined by the property

$$E(H)=\sum_{i=1}^{n} w_i[H(X_i,Y_i)-Z_i]^2 + E_{\text{curvature}}(H)\ \text{minimal}, \quad (10)$$

the weights w_i regulate not only the importance given to each point (X_i,Y_i,Z_i) with respect to the others, but also the importance of the sampling fitting criterion E_{sample} with respect to the curvature criterion $E_{\text{curvature}}$. To separate these two roles, we prefer to write

$$E(H)=\lambda\sum_{i=1}^{n} \mu_i[H(X_i,Y_i)-Z_i]^2 + E_{\text{curvature}}(H)\ \text{with}\ \sum_{i=1}^{n}\mu_i=1. \quad (11)$$

λ regulates the importance of the $\sum_i \mu_i(H(X_i,Y_i)-Z_i)^2$ criterion with respect to $E_{\text{curvature}}$; the choice of λ is done manually by comparing the lengths of initial contours with the interpolated DTM contours (see Section 4). However, the experience shows that for $\lambda\in[10^3,10^5]$, the elastic grid method gives acceptable results (Gonçalves, 1999). So from now we consider its value to be fixed, and we worry about the relative weights μ_i.

In the context of this paper, the set S is formed by points sampled from the CLs (eventually enriched by additional points, see Section 3). The most straightforward choice is to assign the same weight μ_i to all points. This is however not satisfying, since the sample points distribution will be heterogeneous, due to the irregular distribution of the contours. Assigning the same weight to all points would make the fitting function H to deflect towards the finely sampled parts of the terrain.

To avoid this inconvenience, the weights μ_i should be smaller in regions where the sample distribution is dense, and higher in regions where it is sparse. In

other words, a weight μ_i must be small when the point $p_i=(X_i,Y_i)$ is representative of a small region V_i and high when it is representative of a large one. This leads us to think that μ_i is an increasing function of area A_i of V_i: $\mu_i=f(A_i)$. On the other hand, this function f has to be additive, because if we aggregate two contiguous regions V_i,V_j into a single one $V_i \cup V_j$, the weight of this composed region must be the sum of the weights: $f(A_i+A_j)=\mu_i+\mu_j=f(A_i)+f(A_j)$. We thus have $\mu_i=\kappa A_i$, and the normalization condition $\sum\mu_i=1$ implies $\kappa=1/\sum A_i$.

It remains to define what the region V_i represented by point p_i is. It is natural to define it as the set of points p closer to p_i than to any other point p_j. This set is known to be a polygonal region V_i, and the family $\{V_i;\ i=1,\ldots,n\}$ forms the "Voronoi diagram" associated to the point set.

To conclude, a coherent weight system w_i can be defined by:

$$w_i = \lambda \frac{A_i}{\sum_{j=1}^{n} A_j} \tag{12}$$

where A_i is the area of polygon V_i.

2.4. Minimizing the criterion E(H)

Expanding Eq. (11) shows $E(H)$ to be a quadratic functional $J(z)$ of $z=(z_{1,1},\ldots,z_{N,1},\ z_{1,2},\ldots,z_{N,2},\ldots,z_{1,M},\ldots,z_{N,M})^T$. In matrix notation, this functional can be written as $J(z)=z^T\Lambda z-2\boldsymbol{b}^T z+d$, where: Λ is a positive, symmetrical, square and sparse matrix of order NM, whose non-zero elements are computed from the grid nodes coordinates and from the weights w_i of the sample points; $\boldsymbol{b}$ is a vector whose NM elements are computed from the grid nodes coordinates of the sample points and from Z_i and the weights w_i of these points; d is a scalar computed from the heights Z_i and from the weights w_i.

It can be shown that Λ is positive-definite if three points exist in the sample that define a non-vertical plan (Gonçalves, 1999); this condition is always verified. Λ is thus invertible, and the identity $J(z)=(z-\Lambda^{-1}\boldsymbol{b})^T\Lambda(z-\Lambda^{-1}\boldsymbol{b})+d-\boldsymbol{b}^T\Lambda^{-1}\boldsymbol{b}$ shows that $J(z)$ reaches the minimal value $d-\boldsymbol{b}^T\Lambda^{-1}\boldsymbol{b}$ when $z-\Lambda^{-1}\boldsymbol{b}=0$, or $\Lambda z=\boldsymbol{b}$. We solve the equation $\Lambda z=\boldsymbol{b}$ using the conjugate gradient method (Ciarlet, 1994).

At this point, we check whether the constraints in Eq. (9) are satisfied. For each grid point (c,l) where they are not satisfied, we add a new sample point (X_c,Y_l,Z_P) such that $Z_1(c,l)\le Z_P\le Z_2(c,l)$, with a weight w_P sufficiently big to force the surface to go through the point; we then solve the new equation $\Lambda z=\boldsymbol{b}$. We repeat this operation until the surface satisfies all the inequality constraints.

3. Solving the intermediate contour problem: constraints on ridges and drainages

3.1. Overview

In Section 1, we have seen that a necessary condition for solving the intermediate contour problem was to constrain the surface by adding supplementary

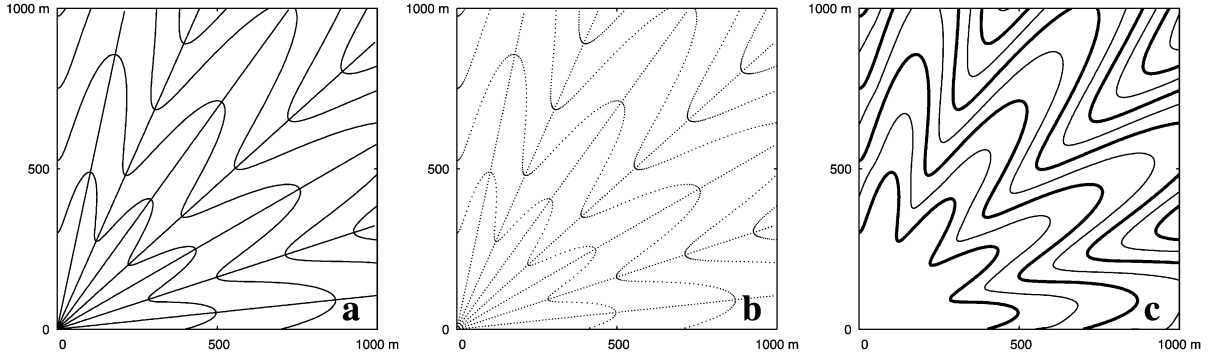

Fig. 2. A solution to the intermediate contours problem. (a) Initial contours with ridge and drainage lines; (b) sample points; (c) initial (in bold) and intermediate contours of the fitted surface.

information. The most straightforward idea is to constrain the surface by adding new points to the initial sample in the regions of the surface where the problem arises, that is, at some morphologic lines (ridges and drainages); the heights of these points must naturally verify the regular slope condition between contour lines. Experience proves this idea to be well founded, as can be seen in Fig. 2, where we use the same synthetic surface as in Fig. 1. Fig. 2a shows the initial contours with ridge and drainage lines added and Fig. 2b shows the point sample; finally in Fig. 2c, we have the CLs computed on the fitted surface. It can be seen that the intermediate lines are now coherent with the initial ones, giving evidence that adding sample points on ridge and drainage lines is enough to obtain a correct surface.

Observe that supplementary information could be added to the $E_{\text{curvature}}$ criterion, instead of E_{sample}; one such attempt is given in Bignone and Nonin (1995), where $E_{\text{curvature}}$ is enhanced to model the erosion of natural landforms. However, its mathematical study becomes more complex.

We prefer keeping the first idea, given its effectiveness (see Fig. 2) and the fact that it can immediately be applied without requiring any modifications to our method. The remaining problem is of course how to obtain the additional points on morphologic lines, from the contour lines only. This is however a problem for which solutions have already been proposed in the literature (see below).

3.2. Automatic extraction of ridge and drainage lines from contours

The ridges and drainages are implicitly contained in the contour lines: they correspond approximately to the strips where the surface has higher curvature than elsewhere. In a topographic map, these are imaginary lines connecting points of maximal curvature. Among the published automatic extraction methods, we may distinguish three categories.

- Methods that connect points of maximal curvature in consecutive contours (Brandli and Schneider, 1994); two consecutive contours may only be connected by line segments, and thus connecting two contours is only possible (without intersecting one of them) if the crest and valley are approximately straight; these methods fail for curved crests and valleys.
- Methods based on slope direction (aspect) estimation. These use an auxiliary surface, defined by a constrained triangulation, to interpolate the aspect

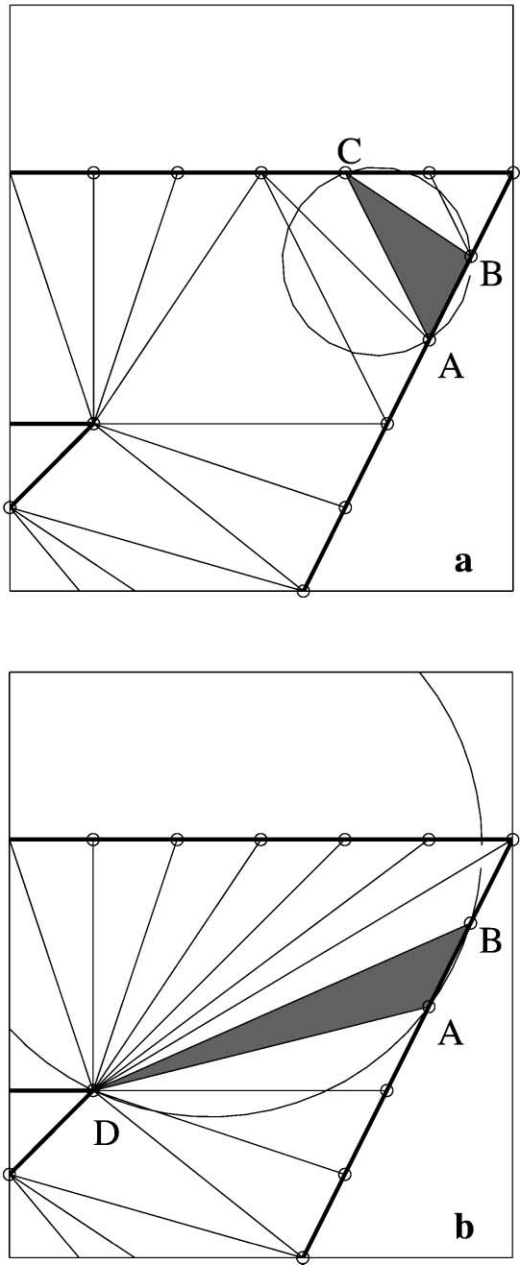

Fig. 3. Properties of triangles in ridge and drainage regions. (a) The horizontal triangle ABC is part of the Delaunay triangulation; (b) ABD is not a possible triangle for the Delaunay triangulation.

between contours. In Aumann et al. (1991), the skeleton lines (ridges and drainages) are built step by step following an estimated aspect; the drawback is that the slope direction is difficult to interpolate in ridge and drainage regions where the triangles are horizontal.

- Medial axis-based methods. These use the notion of a medial axis to find the morphologic lines in a raster contour line image (Tang, 1992); ridges and drainages will correspond to the portions of the axis located between the two parts of the same contour; this technique has the inconvenience that it requires a higher resolution of the contour image to produce acceptable results.

3.2.1. Proposal of a new method based on the notion of medial axis

Our approach also makes use of an auxiliary surface, defined by a Delaunay triangulation built from a particular set of points sampled from the CLs. It is based on (and takes advantage of) the fact that ridges and drainages are characterized by the presence of horizontal triangles. Indeed, we know this triangulation to satisfy the empty circumcircle criterion, i.e., that the circumcircle of a triangle contains no other triangle vertex. Let us then examine in Fig. 3 what takes place on a ridge or drainage. We see that any triangle such as *ABD* connecting two different contours is impossible since the circle *ABD* contains other points than *A*, *B*, *D*; *ABC* on the other hand is a possible triangle.

The above arguments implicitly assume that the vertices of any triangle are either on the same contour, or on two contours, but never on three contours. This is so if this is a conforming triangulation, that is, if it contains segments (and/or portions of these) of the graph formed by the contours. A method for obtaining such a triangulation is given in Shewchuk (1996).

The basic principle of the method is then to find the medial axis of each polygon resulting from merging a set of contiguous horizontal triangles. The medial axis of a planar region enclosed by a single polygonal chain

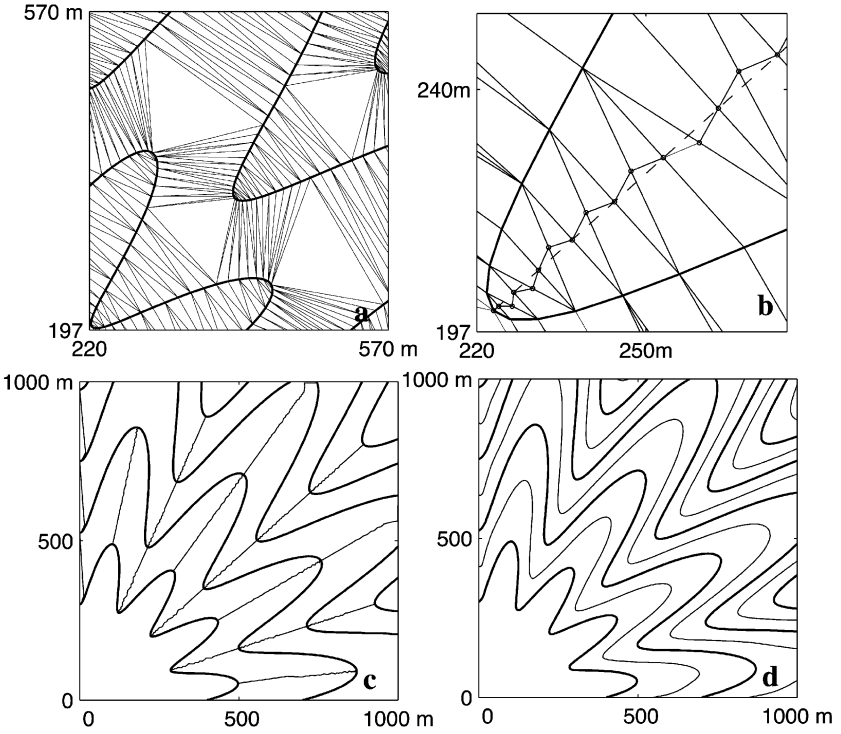

Fig. 4. Automatic extraction of constraint lines from CLs: (a) detail of the Delaunay triangulation conform to CLs; (b) detail of an estimated medial axis (solid line), and a true medial axis (dashed line); (c) CLs and estimated medial axes resulting from our approach; (d) initial (in bold) and intermediate contours of the interpolated elastic grid DTM.

C is the set of points s interior to C that have more than one closest point among the points of C; this axis is in general a tree line. Once it has been computed, this axis is adopted as a ridge or drainage line.

For our purposes, we have no need to find the exact medial axis. It is enough to approximate it by the polygonal line connecting the midpoints in the common sides of two triangles. This line is finished at each extremity by the segment that connects it to the opposed vertex in the triangle where the line terminates (see Fig. 4b). Therefore, such a medial line always connects two contours. It remains to assign the height of the points in the medial line: we interpolate linearly by arc length. In the case where several medial lines meet, we first compute the heights in the longest line (that we take to be the main line), and then in the remaining branches.

Fig. 4 illustrates the main steps in this procedure. Fig. 4a shows a detail of the conforming Delaunay triangulation; we compute this triangulation using the method described in Shewchuk (1996). Fig. 4b shows a detail of an estimated medial axis (solid line), and the true medial axis (dashed line). Fig. 4c is a global view of the CLs and the estimated medial axes; one can see that these axes are good approximations to the ridge and drainage lines. Fig. 4d shows the CLs in the interpolated surface constrained by these lines, with correct intermediate contours.

3.3. Experimental results for real terrain

In Fig. 5, we show the implementation of the principles given above, for the case of real terrain. Fig. 5a shows the initial contours with a 5-m contour interval obtained by photogrammetric survey. We have extracted a representative sample from the contours, and fitted a surface to it using the elastic grid method. Fig. 5b represents the 1-m contour lines of

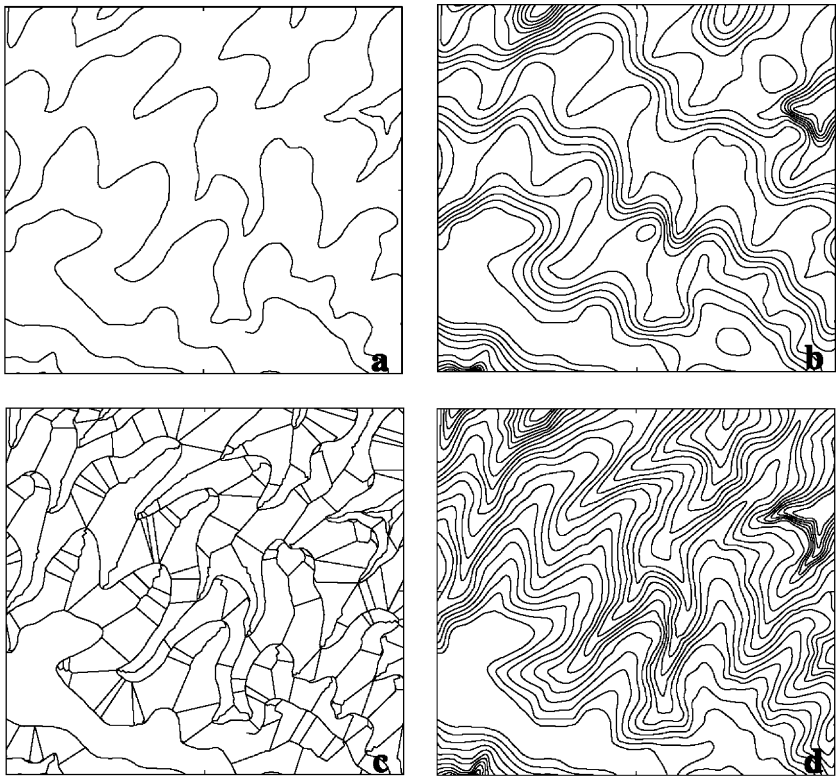

Fig. 5. Application to a real terrain (2600 by 2400 m in size). (a) Initial CLs; (b) DTM contours without constraint lines; (c) initial CLs with constraint lines; (d) DTM contours using constraint lines.

the fitted surface, with the intermediate contours too tight (not matching the initial contours); these intermediate contours represent irregular terrain slopes between the initial contours, failing to satisfy the modelling contour line principle. Fig. 5c shows the "constraint lines" obtained by a triangulation conforming to the initial contours (some of these lines approach the ridge and drainage lines). On these lines, we have sampled an additional set of points. We have then fitted a surface to the global sample by the elastic grid method. Fig. 5d shows the resulting contour lines. The intermediate contours now perfectly match the initial contours so much that they become indiscernible.

4. Evaluation of the coherence between initial and intermediate contours

We now complement the visual evaluation of the quality of intermediate contours, by a numerical evaluation. The fact that the incorrect intermediate contours appear to be tighter, thus shorter than the initial ones, suggests that criteria such as the "mean curvature" or the length of the contours should be able to detect these artifacts.

This is confirmed by Fig. 6, where we give the contour length graphs. Fig. 6a corresponds to an incorrect surface; we see the length irregularity at the initial contours compared to the intermediate ones; furthermore, the "U" shape between two initial contours shows that the farther the intermediate contours are from the initial ones, the less their lengths match. Fig. 6b corresponds to a correct surface; lengths are visibly more regular, as expected. In the case of perfectly linear interpolation between contour lines, we can even expect to obtain a piecewise linear graph. In fact, the terrain can be locally assimilable to a cone section where the length of the contours varies linearly with height. Notice however that the interpolator is not linear, since the elastic grid performs a smoother interpolation between contours. We will thus obtain a smoother graph than a piecewise linear one.

5. Conclusions

The results, which we find satisfying, obtained for real terrain, show that adding supplementary points (sampled from the morphologic lines) to the initial set of points (sampled from the CLs) is a possible solution to the intermediate contours problem. Further improvements should refine the morphologic line extraction procedure. For instance, in the case of asymmetrical crests and valleys, the morphologic line is not a medial axis; it is slightly deflected towards the steepest side. Furthermore, one might extract these lines directly from a Voronoi diagram, where they are particularly visible. However, this proposition disagrees with the previous one.

In addition, the contour length seems to be an appropriate criterion to detect the slope-related arte-

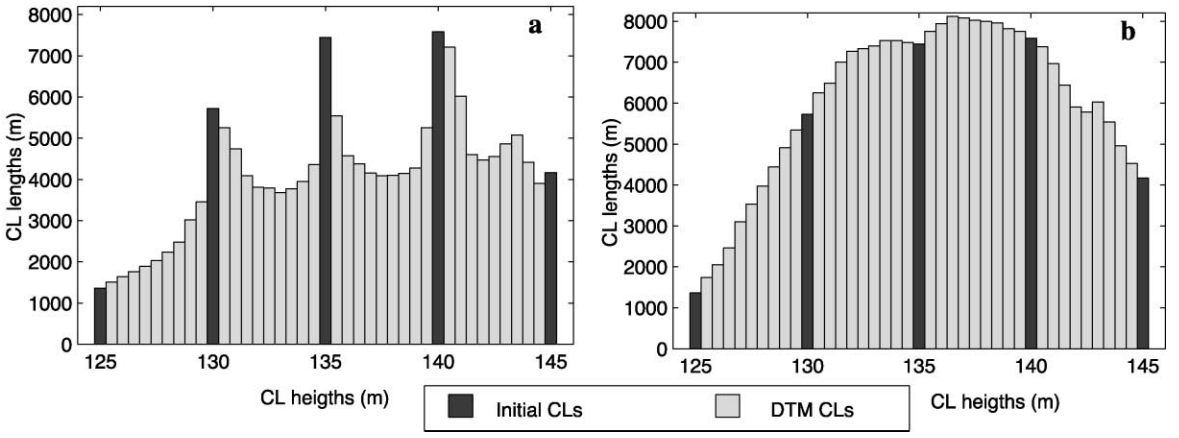

Fig. 6. Coherence evaluation between initial and intermediate contours: (a) CL length for the DTM in Fig. 5b; (b) CL length for the DTM in Fig. 5d.

facts in a DTM. We have also tested the mean curvature criterion. Our first experiments (Gonçalves, 1999) show that this is a very fine criterion, revealing artefacts even for the acceptable DTM of Fig. 5d. This criterion seems to be able to detect ''higher-order'' artefacts in DTMs, but this is beyond our cartographic needs.

Acknowledgements

This work was partially supported by Fundação para a Ciência e Tecnologia, Portugal (FCT) grant No. PRAXIS XXI BD-5339-95.

Appendix A. Error upper bond for the cubic interpolation

Let $f(x)$ be a sampled function at equally spaced interpolation nodes x_c (c=1,...,n), and let

$$g(x) = \sum_{c=1}^{n} f(x_c) V_a\left(\frac{x - x_c}{h}\right) \tag{A.1}$$

be the interpolation function. We want to estimate an upper bound for the interpolation error

$$\epsilon = \| g - f \| = \sup_{[x_1, x_n]} |\, g(x) - f(x) \,|. \tag{A.2}$$

In a neighborhood of x_c, we approximate f by its third-order Taylor expansion:

$$f(x) = f(x_c) + f'(x_c)sh + \frac{1}{2}f''(x_c)s^2h^2 + \frac{1}{6}f'''(x_c)s^3h^3$$

$$f(x_{c-1}) = f(x_c) - f'(x_c)h + \frac{1}{2}f''(x_c)h^2 - \frac{1}{6}f'''(x_c)h^3$$

$$f(x_{c+1}) = f(x_c) + f'(x_c)h + \frac{1}{2}f''(x_c)h^2 + \frac{1}{6}f'''(x_c)h^3$$

$$f(x_{c+2}) = f(x_c) + f'(x_c)2h + \frac{1}{2}f''(x_c)2^2h^2 + \frac{1}{6}f'''(x_c)2^3h^3 \tag{A.3}$$

where $s=(x - x_c)/(h)$, and f', f'' and f''' the first, second and third derivatives, respectively.

Let $x \in [x_c, x_{c+1}]$, then $0 \le s \le 1$. Since V_a is zero except inside the interval $[-2, +2]$, Eq. (A.1) reduces to at most four non-zero terms:

$$g(x) = f(x_{c-1})V_a(s+1) + f(x_c)V_a(s) + f(x_{c+1})V_a(s-1) + f(x_{c+2})V_a(s-2). \tag{A.4}$$

By substituting Eq. (A.3) into the above relationship and collecting powers of s, it follows that:

$$\begin{aligned} g(x) - f(x) = {} & hf'(x_c)[(2a+1)(-2s^3 + 3s^2 - s)] \\ & + \frac{1}{2}h^2 f''(x_c)[(4a+2)(-s^3 + s^2)] \\ & + \frac{1}{6}h^3 f'''(x_c)[-(10a+3)s^3 \\ & + (12a+3)s^2 - 2as]. \end{aligned} \tag{A.5}$$

In particular, this equation shows that the interpolation error is 0 when $a=-1/2$ and f is a polynomial of degree ≤ 2.

Since $0 \le s \le 1$, the polynomials in Eq. (A.5) are bounded, thus we have:

$$\begin{aligned} |\, g(x) - f(x) \,| \le {} & h\,|f'(x_c)|\;\;|\,2a+1\,|\,S_1 \\ & + \frac{h^2}{2}\,|f''(x_c)|\;\;|\,4a+2\,|\,S_2 \\ & + \frac{h^3}{6}\,|f'''(x_c)|\,(S_1 + |\,2a+1\,|\,S_3) \end{aligned} \tag{A.6}$$

with

$$|\, -2s^3 + 3s^2 - s \,| \le S_1;\; |\, -s^3 + s^2 \,| \le S_2;$$
$$|\, -5s^3 + 6s^2 - s \,| \le S_3.$$

Further, if f', f'', f''' are bounded over $\mathbf{R}=[-\infty, +\infty]$ then

$$\epsilon \le \begin{cases} Ch^3 & \text{if } a = -1/2 \\ Ah & \text{if } a \neq -1/2 \end{cases} \tag{A.7}$$

where $C=(\|f'''\|)/(6)\ S_1$,

$$A = \|f'\|\ |2a+1|\,S_1 + \frac{h}{2}\|f''\|\ |4a+2| + \frac{h^2}{6}\|f'''\|\,(S_1 + |2a+1|\,S_3)$$

and $\|f\|$ denotes $\sup\{|f(x)|;\ x\in\mathbf{R}\}$.

Since $\sup_{[0,1]}|2s^3-3s^2+s|=1/(6\sqrt{3})$, and since for small h, $A \approx |2a+1|\ \|f'\|\ S_1$, then:

$$\epsilon \le \begin{cases} \frac{\|f'''\|}{36\sqrt{3}}h^3 & \text{if } a=-1/2 \\ |2a+1|\,\frac{\|f'\|}{6\sqrt{3}}h & \text{if } a\neq -1/2 \end{cases}. \qquad \text{(A.8)}$$

Note that, for $a\neq -1/2$ the inequality (Eq. (A.8)) cannot be improved (i.e., there is no inequality $\epsilon \le Ah^2$ valid for all functions f), since if $f(x)=x$, for example, we have the equality $\epsilon = \frac{|2a+1|}{6\sqrt{3}}h$.

Finally, Eq. (A.8) shows that for $a=-1/2$, $U=V_{-1/2}$ gives an interpolation error that goes to zero at least as fast as h^3, that is an $O(h^3)$ error or convergence rate as in Keys (1981); any other V_a gives an $O(h)$ error.

References

Aumann, G., Ebner, H., Tang, L., 1991. Automatic derivation of skeleton lines from digitized contours. ISPRS Journal of Photogrammetry and Remote Sensing 46 (5), 259–268.

Bignone, F., Nonin, P., 1995. Une amélioration de la métode spline plaque-mince en vue du calcul de modèles numériques de terrain. Bulletin de la Société Française de Photogrammétrie et Télédétection 139, 20–31.

Brandli, M., Schneider, B., 1994. Shape modeling and analysis of terrain. International Journal of Shape Modeling 1 (2), 167–189.

Ciarlet, P., 1994. Introduction à l'analyse numérique matricielle et à l'optimisation Masson, Paris.

D'Autume, G.M., 1978. Construction du modèle numérique d'une surface par approximations successives: applications aux modèles numériques de terrain. Bulletin de la Société Française de Photogrammétrie et Télédétection 71, 33–41.

Duchon, J., 1976. Interpolation des fonctions de deux variables suivant le principe de la flexion des plaques minces. Revue Française d'Automatique. Informatique et Recherche Opératonnelle Analyse Numérique 10 (12), 5–12.

Gonçalves, G., 1999. Qualités requises en modélisation numérique du relief: étude de l'equivalence entre le modèle cartographique et le modèle numérique. PhD Thesis, Université de Marne-la-Vallee.

Grimson, W., 1981. From Images to Surfaces: A Computational Study of the Human Early Vision MIT Press, Cambridge, MA.

Julien, P., 1994. Traitements altimétriques: modèles numériques de terrain. Cours du DEA des Sciences de l'Information Géographiques (Lecture Notes), Institut Géographique National.

Keys, R.G., 1981. Cubic convolution interpolation for digital image processing. IEEE Transactions on Acoustics, Speech, Signal Processing ASSP 29 (6), 1153–1160.

Robinson, G., 1994. The accuracy of digital elevation models derived from digitised contour data. Photogrammetric Record 14 (83), 805–814.

Shewchuk, J., 1996. Triangle: engineering a 2d quality mesh generator and Delaunay triangulator. Proc. First ACM Workshop on Applied Computational Geometry, pp. 124–133.

Tang, L., 1992. Automatic extraction of specific geomorphological elements from contours. Proc. 5th Int. Symp. on Spatial Data Handling, vol. 2, pp. 554–566.